

General framework for acoustic emission during plastic deformationJagadish Kumar,¹ Ritupan Sarmah,² and G. Ananthakrishna³¹*Department of Physics, Utkal University, Bhubaneswar 751004, India*²*Department of Physics, Tezpur University, Tezpur-784028, India*³*Materials Research Centre, Indian Institute of Science, Bangalore 560012, India*

(Received 23 April 2015; revised manuscript received 13 August 2015; published 20 October 2015)

Despite the long history, so far there is no general theoretical framework for calculating the acoustic emission spectrum accompanying any plastic deformation. We set up a discrete wave equation with plastic strain rate as a source term and include the Rayleigh-dissipation function to represent dissipation accompanying acoustic emission. We devise a method of bridging the widely separated time scales of plastic deformation and elastic degrees of freedom. While this equation is applicable to any type of plastic deformation, it should be supplemented by evolution equations for the dislocation microstructure for calculating the plastic strain rate. The efficacy of the framework is illustrated by considering three distinct cases of plastic deformation. The first one is the acoustic emission during a typical continuous yield exhibiting a smooth stress-strain curve. We first construct an appropriate set of evolution equations for two types of dislocation densities and then show that the shape of the model stress-strain curve and accompanying acoustic emission spectrum match very well with experimental results. The second and the third are the more complex cases of the Portevin-Le Chatelier bands and the Lüders band. These two cases are dealt with in the context of the Ananthakrishna model since the model predicts the three types of the Portevin-Le Chatelier bands and also Lüders-like bands. Our results show that for the type-C bands where the serration amplitude is large, the acoustic emission spectrum consists of well-separated bursts of acoustic emission. At higher strain rates of hopping type-B bands, the burst-type acoustic emission spectrum tends to overlap, forming a nearly continuous background with some sharp acoustic emission bursts. The latter can be identified with the nucleation of new bands. The acoustic emission spectrum associated with the continuously propagating type-A band is continuous. These predictions are consistent with experimental results. More importantly, our study shows that the low-amplitude continuous acoustic emission spectrum seen in both the type-B and type-A band regimes is directly correlated to small-amplitude serrations induced by propagating bands. The acoustic emission spectrum of the Lüders-like band matches with recent experiments as well. In all of these cases, acoustic emission signals are burstlike, reflecting the intermittent character of dislocation-mediated plastic flow.

DOI: [10.1103/PhysRevB.92.144109](https://doi.org/10.1103/PhysRevB.92.144109)

PACS number(s): 43.40.Le, 62.20.fq, 05.45.-a, 83.50.-v

I. INTRODUCTION

Two striking features of acoustic emission are its intermittent character and its occurrence in a surprisingly large variety of systems, ranging from geological scales to laboratory scales. A good example from the geological scale is the acoustic emission (AE) during volcanic activity [1]. Varied laboratory scale examples such as AE from crack nucleation and propagation in fracture of solids [2–4], thermal cycling of martensites [5–7], peeling of an adhesive tape [8–11], and collective dislocation motion [12–14] can be cited. Clearly, while the sources that lead to AE signals in such widely different situations are necessarily different, they are generally attributed to the release of stored elastic energy in the system. Further, the AE spectrum in all of these cases is intermittent, a feature reflective of the underlying jerky motion of the sources generating the AE signals. The phenomenon has been effectively used as a nondestructive tool in locating the sources and mechanisms generating the AE signals [15]. The method involves recording the arrival times of a wave at multiple transducers which, in turn, determines the distances of the AE source from the transducers. This procedure is akin to that adopted in fracture studies on rock samples [2,13]. This method has been used to explain the power-law distribution of the amplitudes of the AE signals in the deformation studies of ice samples [12,13].

Considerable insight into the intermittent character of dislocation-mediated plastic deformation has come from acoustic emission measurements [12,13,15]. Indeed, such AE

studies carried out for over five decades have established specific correlations between the nature of the AE signals and the stress-strain curves for different situations [16–24]. However, there is lack of clarity as to why such distinct correlations exist [16–22,25]. For instance, even early studies on the AE spectrum for the smooth homogeneous yield phenomenon showed an intermittent AE spectrum [16]. Improved techniques confirm the pulselike character of the AE events. The general shape of the AE spectrum for this case exhibits a peak just beyond the elastic regime decaying for larger strains [16,19]. Since the stress-strain ($\sigma - \epsilon$) curves remain smooth, the pulselike acoustic emission signals are attributed to the intrinsic intermittent motion of dislocations. Then, the smooth $\sigma - \epsilon$ curves are interpreted as resulting from the averaging process of the dislocation activity in the sample. Indeed, the intermittent character of dislocation motion at the microscopic level is reflected in the strong stress fluctuations seen in nanometer-sized samples that are not seen in macroscopic samples [26].

In contrast, the nature of the AE spectrum is qualitatively different for the case of discontinuous flows where the stress-strain curves display stress serrations. For example, studies of the Portevin-Le Chatelier (PLC) effect, a kind of propagative instability, have established specific types of correlations between the AE spectrum and the different types of deformation bands and the associated stress-strain curves [17,20–22,25]. Similar correlations exist for the Lüders band [21–24], another

type of propagative instability [27]. Furthermore, the AE spectrum for the Lüders band [27] is different from that for the three types of PLC bands [28,29]. In these cases of propagative instabilities, collective dislocation processes govern the nature of the bands and the associated stress-strain curves. Thus, there is a necessity to simultaneously describe the collective behavior of dislocations and the wave equation that captures the inertial time scale.

Early theoretical attempts to explain AE during plastic deformation were based on the AE response of individual dislocation mechanisms such as the Frank-Reed source [30–32]. However, such methods are clearly unsuitable while following the AE signals during the entire course of deformation since the AE sources themselves evolve as dislocations multiply and interact with each other. Clearly, the AE spectrum from collective dislocation phenomena such as the PLC effect and Lüders band cannot be explained as a superposition of individual dislocation contributions.

The purpose of the present paper is to set up a general mathematical framework for describing the acoustic emission for *any type* of plastic deformation. Devising such a theory involves developing a method for dealing with widely separated time scales of plastic deformation and the inertial time scale, and a method for describing collective effects of dislocations manifested in the PLC effect and Lüders bands [28,33–37]. In a preliminary short communication, we outlined a way of dealing with both dislocation dynamics and elastic degrees of freedom specifically applicable to the PLC instability [14]. Our present approach involves several mathematical steps such as (a) including a dissipative term representing the acoustic energy, (b) using the plastic strain rate as a source term in the wave equation for the elastic degrees of freedom, (c) setting up evolution equations for dislocation microstructure, and (d) imposing mutually compatible boundary conditions on both the wave equation and the evolution equations for the dislocation microstructure. As we shall show, point (d) requires describing the wave equation at a discrete level.

Consider the functional form for the dissipated acoustic energy in terms of a relevant “state variable” that also evolves as deformation proceeds. To be applicable to any plastic deformation, we require the functional form for the dissipated AE energy to be independent of the nature of the deformation process or the evolving microstructure, but such that it could be coupled to the evolution equations for the dislocation microstructure. Indeed, an expression for the dissipated acoustic energy was introduced while modeling the power-law distribution of AE signals during thermal cycling of martensites [6,7]. The idea was that, to a leading order, dissipated acoustic energy could be represented by the Rayleigh-dissipation function [38]. This choice proved quite successful in explaining the AE spectrum in a number of situations, including the power-law distribution of the AE signals during martensite transformation [6,7], peeling of an adhesive tape [10,11], and crack propagation [4]. However, in these cases, only elastic or viscoelastic degrees of freedom having similar order time scales had to be described. In contrast, plastic deformation is more complicated since it requires describing widely separated time scales of plastic deformation and inertial time scale.

The efficacy of the framework is illustrated for three cases. First is the acoustic emission during a continuous yield, second is during the PLC bands, and the third is during the Lüders band. For the first case, we set up a dislocation dynamical model that uses two types of dislocation densities to predict the smooth stress-strain curve and also the general shape of the AE spectrum and its burstlike character. For the second and third cases, we use the Ananthakrishna (AK) model for the PLC effect [39] since it predicts the most generic features of the PLC effect including the three band types [33,34,36,37,39] and also Lüders-like bands [37]. The AE bursts for the uncorrelated type-C bands are well separated as the type-C stress drops. For the hopping type-B bands, the AE bursts overlap, forming low-amplitude nearly continuous background AE signals. More importantly, we find sharp bursts of AE superposed on the low-level continuous AE background that can be unambiguously identified with the nucleation of new bands. For the type-A propagating band, we find a continuous AE spectrum. All of these features are consistent with the experimental AE spectrum [20–22]. For the Lüders band, the nature of the AE spectrum predicted is again consistent with recent experiments [21–23].

II. A GENERAL FRAMEWORK FOR ACOUSTIC EMISSION DURING PLASTIC DEFORMATION

We begin by constructing a wave equation that includes the contribution from dissipated acoustic energy. For the sake of simplicity, we work in one dimension. The physical mechanism attributed to the generation of AE signals during plastic deformation can be broadly termed “dislocation multiplication mechanisms” such as the Frank-Reed source, the abrupt unpinning of dislocations from pinning points, or from solute atmosphere as in the case of the PLC effect. These mechanisms set off local elastic disturbances. There are dissipative forces that tend to oppose the growth of the elastic disturbances so that mechanical equilibrium is restored. We represent the dissipative energy [4,6,7,10,11] by the Rayleigh-dissipation function [38] given by $\mathcal{R}_{AE} = \frac{\eta}{2} \int \left[\frac{\partial \dot{\epsilon}_e(y)}{\partial y} \right]^2 dy$. Here, η is the damping coefficient. Noting that $\mathcal{R}_{AE} \propto \dot{\epsilon}_e^2(t)$, we interpret \mathcal{R}_{AE} as the acoustic energy that is dissipated during the abrupt motion of dislocations [4,6].

We now set up the wave equation for the elastic strain ϵ_e for a one-dimensional crystal. The Lagrangian consists of the kinetic energy of the crystal $T = \frac{\rho}{2} \int \left[\frac{\partial \epsilon_e(y)}{\partial t} \right]^2 dy$ with ρ referring to the density of the material, the strain energy $V_{loc} = \frac{\mu}{2} \int \left[\frac{\partial \epsilon_e(y)}{\partial y} \right]^2 dy$ with μ referring to the elastic constant, and the gradient energy $V_{grad} = \frac{D}{4} \int \left[\frac{\partial^2 \epsilon_e(y)}{\partial y^2} \right]^2 dy$ where D is the strain gradient coefficient. V_{grad} makes the sound wave dispersive, a term that is particularly important when localized transient waves are generated. This term may be regarded as the next dominant term (to the strain energy) in the Ginzburg-Landau expansion of the free energy. Then, using the Lagrangian $\mathcal{L} = T - V_{loc} - V_{grad}$ in the Lagrange equations of motion,

$$\frac{d}{dt} \left[\frac{\delta \mathcal{L}}{\delta \dot{\epsilon}_e(y)} \right] - \frac{\delta \mathcal{L}}{\delta \epsilon_e(y)} + \frac{\delta \mathcal{R}}{\delta \dot{\epsilon}_e(y)} = 0, \quad (1)$$

we have

$$\rho \frac{\partial^2 \epsilon_e}{\partial t^2} = \mu \frac{\partial^2 \epsilon_e}{\partial y^2} + \eta \frac{\partial^2 \dot{\epsilon}_e}{\partial y^2} - D \frac{\partial^4 \epsilon_e}{\partial y^4}. \quad (2)$$

Equation (2) describes sound waves in the absence of dislocations. However, during plastic flow, transient elastic waves (or acoustic emission) are triggered by the abrupt motion of dislocations, which then propagate through the elastic medium. This can be described by including plastic strain rate as a source term in Eq. (2). Then, the relevant (inhomogeneous) wave equation describing the acoustic emission process takes the form

$$\rho \frac{\partial^2 \epsilon_e}{\partial t^2} = \mu \frac{\partial^2 \epsilon_e}{\partial y^2} - \rho \frac{\partial^2 \epsilon_p}{\partial t^2} + \eta \frac{\partial^2 \dot{\epsilon}_e}{\partial y^2} - D \frac{\partial^4 \epsilon_e}{\partial y^4}. \quad (3)$$

Here, $c = \sqrt{\mu/\rho}$ is the velocity of sound and $\dot{\epsilon}_p(y, t)$ is the plastic strain rate. Note that $\dot{\epsilon}_p(y, t)$ is a function of both space and time and hence contains full information of any heterogeneous character of the deformation (as for the PLC effect), which has to be calculated by setting up appropriate evolution equations for suitable types of dislocation densities.

We note here that Eq. (3) has the standard form of a partial-differential equation with $\dot{\epsilon}_p$ acting as a source term. This form excludes the possibility of transient acoustic waves (generated by the source $\dot{\epsilon}_p$ itself) influencing the plastic strain rate or, equivalently, dislocations or collective dislocation motion as the case may be. Such an effect is, at best, a second-order effect.

Finally, we need to specify the initial and boundary conditions of Eq. (3). First, the constant strain rate condition is imposed by fixing one end of the sample and applying a traction at the other end. Second, the boundary conditions of Eq. (3) should be consistent with those imposed on the evolution equations for the dislocation densities, in which the latter is determined by physically meaningful values for the dislocation densities. Then, $\dot{\epsilon}_p(y, t)$ obtained near the boundary sites need not be consistent with those imposed on Eq. (3). Third, the machine stiffness gripping the ends of the sample is higher than that of the sample, which is not easy to include in Eq. (3). In fact, conventionally, the information about the machine stiffness (for example, in the constant strain rate case) goes only in the effective modulus of the machine and the sample. Therefore, we start with a Lagrangian defined on a grid of N points and derive a discrete set of wave equations. This method allows us to make a distinction between points well within the sample and those at the boundary where the machine grips the sample. The method also brings clarity to the boundary conditions.

Discrete form of the wave equation

Consider a sample of length L deformed in a constant strain rate condition schematically represented by a spring-block system of N points of mass m coupled to each other through spring constant k_s , as shown in Fig. 1. Then, the condition that the sample is gripped at the ends translates into using a different spring constant k_m for the end springs. Let a be the separation between the points in the undistorted state. Then, the local displacements from the equilibrium positions are the dynamical variables of interest. However, since we use plastic

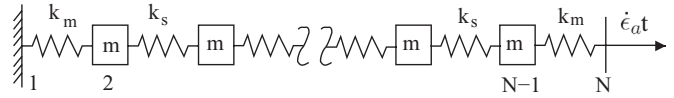


FIG. 1. Mechanical model for the specimen fixed at one end and pulled at a constant strain rate at the other end.

strain rate for describing plastic deformation, we use strain variables. Therefore, we define the strain variables $\epsilon_e(i)$ and their time derivative $\dot{\epsilon}_e(i)$ for each of these points. Further, the condition that the sample is pulled at a constant strain rate is imposed by fixing the first point and pulling the N th point at a constant strain rate $\dot{\epsilon}_a$. Then, we can define a Lagrangian for the system of N points. The kinetic energy T of the system is

$$T = \sum_{i=2}^{N-1} \frac{1}{2} m \dot{\epsilon}_e^2(i). \quad (4)$$

Here the overdot refers to the time derivative. The local potential energies V_{loc} and V_{grad} are, respectively, given by

$$V_{\text{loc}} = \sum_{i=2}^{N-2} \frac{k_s}{2} [\epsilon_e(i+1) - \epsilon_e(i)]^2 + \frac{k_m}{2} \epsilon_e^2(2) + \frac{k_m}{2} [\epsilon_e(N-1) - \epsilon_e(N)]^2, \quad (5)$$

$$V_{\text{grad}} = \sum_{i=3}^{N-2} \frac{D}{2} [\epsilon_e(i+1) + \epsilon_e(i-1) - 2\epsilon_e(i)]^2 + \frac{D}{2} [\epsilon_e(3) - 2\epsilon_e(2)]^2 + \frac{D}{2} \epsilon_e^2(2) + \frac{D}{2} \epsilon_e^2(N-1) + \frac{D}{2} [\epsilon_e(N) - 2\epsilon_e(N-1) + \epsilon_e(N-2)]^2. \quad (6)$$

The dissipated acoustic energy is given by

$$R_{AE} = \frac{\eta}{2} \sum_{i=2}^{N-2} [\dot{\epsilon}_e(i+1) - \dot{\epsilon}_e(i)]^2 + \frac{\eta}{2} [\dot{\epsilon}_e^2(2) + \dot{\epsilon}_e^2(N-1)]. \quad (7)$$

Then, using the Lagrange equations of motion, we get

$$\ddot{\epsilon}_e(1) = 0, \quad (8)$$

$$\ddot{\epsilon}_e(2) = -\frac{c^2}{a^2} \left[\{\epsilon_e(2) - \epsilon_e(3)\} + \frac{k_m}{k_s} \epsilon_e(2) \right] - \frac{\partial \dot{\epsilon}_p(2, t)}{\partial t} - \frac{\eta'}{a^2 \rho} [\dot{\epsilon}_e(2) - \dot{\epsilon}_e(3)] + \frac{D'}{a^4 \rho} [\epsilon_e(4) + \epsilon_e(2) - 2\epsilon_e(3)], \quad (9)$$

$$\ddot{\epsilon}_e(3) = \frac{c^2}{a^2} [\epsilon_e(4) + \epsilon_e(2) - 2\epsilon_e(3)] - \frac{\partial \dot{\epsilon}_p(3, t)}{\partial t} + \frac{\eta'}{a^2 \rho} \{\dot{\epsilon}_e(4) + \dot{\epsilon}_e(2) - 2\dot{\epsilon}_e(3)\} - \frac{D'}{a^4 \rho} \{\epsilon_e(5) - 4\epsilon_e(4) + 5\epsilon_e(3) - 2\epsilon_e(2)\}, \quad (10)$$

$$\begin{aligned} \ddot{\epsilon}_e(i) = & \frac{c^2}{a^2} \{ \epsilon_e(i+1) - 2\epsilon_e(i) + \epsilon_e(i-1) \} - \frac{\partial \dot{\epsilon}_p(i,t)}{\partial t} \\ & + \frac{\eta'}{a^2 \rho} \{ \dot{\epsilon}_e(i+1) - 2\dot{\epsilon}_e(i) + \dot{\epsilon}_e(i-1) \} \\ & - \frac{D'}{a^4 \rho} [\epsilon_e(i+2) - 4\epsilon_e(i+1) + 6\epsilon_e(i) \\ & - 4\epsilon_e(i-1) + \epsilon_e(i-2)], \end{aligned} \quad (11)$$

$$\begin{aligned} \ddot{\epsilon}_e(N-1) = & -\frac{c^2}{a^2} [\{ \epsilon_e(N-1) - \epsilon_e(N-2) \} \\ & - \frac{k_m}{k_s} \{ \epsilon_e(N) - \epsilon_e(N-1) \}] \\ & - \frac{\partial \dot{\epsilon}_p(N-1,t)}{\partial t} + \frac{\eta'}{a^2 \rho} [\dot{\epsilon}_e(N) + \dot{\epsilon}_e(N-2) \\ & - 2\dot{\epsilon}_e(N-1)] - \frac{D'}{a^4 \rho} [\epsilon_e(N-3) - 4\epsilon_e(N-2) \\ & + 5\epsilon_e(N-1) - 2\epsilon_e(N)]. \end{aligned} \quad (12)$$

Equation (11) is valid for $i = 4$ to $N - 1$. Using $\rho = m/a^3$ and appropriate length factors of a , we retain the definition of $c^2 = \mu/\rho$ [see Eq. (3)] with $\mu = k_s/a$, $\eta' = \eta/a$, and $D' = Da$. Note that $\dot{\epsilon}_p$ has been included as a source term in Eqs. (8)–(12). Equations (8)–(12) are solved on a grid of N points with appropriate initial and boundary conditions. The initial conditions are

$$\epsilon_e(1,0) = 0; \quad \epsilon_e(i,0) = 0 + \xi \times \epsilon_r, \quad i = 2, \dots, N-1, \quad (13)$$

where ϵ_r represents the strain due to inherent defects in the sample and ξ is a random number in the interval $-\frac{1}{2} < \xi < \frac{1}{2}$. Here, we use $\epsilon_r \sim 10^{-7}$. The boundary condition that the left end is fixed and the right end is being pulled at a constant strain rate $\dot{\epsilon}_a$ can be written as

$$\epsilon_e(1,t) = 0, \quad \epsilon_e(N,t) = \dot{\epsilon}_a t; \quad t > 0. \quad (14)$$

III. DISLOCATION DYNAMICAL MODELS FOR PLASTIC DEFORMATION

These steps are clearly applicable to any plastic deformation situation, but must be supplemented by constructing dislocation-based models to calculate the source term $\dot{\epsilon}_p$ in the wave equation. The types of dislocation densities that must be used and the nature of the equations are dictated by the kind of plastic deformation considered, namely the continuous yield and the two propagative instabilities [28,33,34,36,37,39]. The dynamical approach followed here has the ability to use experimental $\dot{\epsilon}_a$, unlike in simulations where the imposed strain rates are several orders of magnitude higher [37]. Further, we can also adopt other experimental parameters used in experiments, for instance σ_y, E^* , etc.

A. A dislocation dynamical model for a continuous yield point phenomenon

We first construct a model that uses two types of dislocation densities, namely, the mobile ρ_m and the immobile (or the

forest) density ρ_{im} that reproduces a typical smooth stress-strain curve. Most dislocation mechanisms used are drawn from the AK model for the PLC effect [28,33–37,39]. They can be broadly categorized into dislocation multiplication and transformation processes. As dislocations multiply (due to the double cross-slip process), they interact with each other to form dipoles and junctions [40]. They can also annihilate. Each of these mechanisms acts as a growth or loss process for ρ_m and ρ_{im} . The general form of multiplication of dislocations can be written as $\theta V_m(\sigma_a) \rho_m$ with $V_m(\sigma_a)$ representing the mean velocity of dislocations. θ is the inverse of a length scale that physically represents points from which the line length of dislocations multiplies (see Refs. [28] and [37] for details). Several phenomenological expressions have been suggested for $V_m(\sigma_a)$ [27]. Here, we use $V_m(\sigma_a) = v_0 \left[\frac{\sigma_{\text{eff}}}{\sigma_m} \right]^m$, where $\sigma_{\text{eff}} = \sigma_a - h \rho_{im}^{1/2}$. Here, m is a velocity exponent and $h \rho_{im}^{1/2}$ is the back stress. The parameter $h = \alpha G b$, where $\alpha \sim 0.3$ is a constant, b is the magnitude of the Burgers vector, and G is the shear modulus. Indeed, one can rewrite the multiplication rate as $v_m \rho_m = v_0 \left[\frac{\sigma_{\text{eff}}}{\sigma_m} \right]^m \rho_m$, where $v_0 = \theta v_0$. The formation of dipoles occurs when two dislocations moving in nearby glide planes approach a minimum distance (typically a few nanometers) and act as a loss term to ρ_m . This is represented by $\beta \rho_m^2$, where β has dimensions of the rate of the area swept out by dislocations. Similarly, the annihilation of a mobile dislocation with an immobile one is represented by the term $f \beta \rho_m \rho_{im}$ with a rate $f \beta$, where f is a dimensionless parameter. This term is generally small compared to other loss terms for ρ_m , and therefore $f \ll 1$. Finally, dislocations moving in different glide planes intersect each other to form junctions. This is a loss term to ρ_m given by $\Theta \rho_m \rho_{im}$. Here, Θ is a parameter that, however, depends on the mean separation between junctions themselves that also evolves as deformation proceeds (i.e., ρ_{im} increases). Then, $\Theta \propto 1/\rho_{im}^{1/2}$ or $\Theta = \delta \rho_{im}^{-1/2}$. Here, δ is considered constant since the main contribution to Θ has been absorbed. Then, the loss term for ρ_m is $\delta \rho_m \rho_{im}^{1/2}$. (δ has the dimension of velocity.) This represents the forest mechanism [40]. This acts as a gain term to ρ_{im} . Then, the evolution equations are

$$\begin{aligned} \frac{\partial \rho_m}{\partial t'} = & \theta v_0 \rho_m \left[\frac{1}{\sigma_y} (\sigma_a - h \rho_{im}^{1/2}) \right]^m - \beta \rho_m^2 - f \beta \rho_m \rho_{im} \\ & - \delta \rho_m \rho_{im}^{1/2} + \frac{\Gamma \theta v_0}{\rho_{im}} \frac{\partial^2}{\partial x^2} \left[\frac{\sigma_{\text{eff}}}{\sigma_y} \right]^m \rho_m, \end{aligned} \quad (15)$$

$$\frac{\partial \rho_{im}}{\partial t'} = \beta \rho_m^2 - f \beta \rho_m \rho_{im} + \delta \rho_m \rho_{im}^{1/2}. \quad (16)$$

(We use the primed time variable for plastic strain rate calculations.) The spatial coupling in Eq. (15) arises since the cross slip allows dislocations to spread into neighboring regions. The factor $1/\rho_{im}$ prevents dislocations from moving into regions of high dislocation density [36].

These equations are coupled to the machine equation [41] that enforces the constant strain rate condition,

$$\begin{aligned} \frac{d\sigma_a}{dt'} = & E^* \left[\dot{\epsilon}_a - \frac{b}{L} \int_0^L v_0 \left(\frac{\sigma_{\text{eff}}}{\sigma_y} \right)^m \rho_m dx \right] \\ = & E^* [\dot{\epsilon}_a - \dot{\epsilon}_p(t')]. \end{aligned} \quad (17)$$

B. The Portevin-Le Chatelier effect and Ananthakrishna model

We first summarize relevant features of the PLC effect [28,29]. The PLC instability is seen in a window of strain rates and temperatures when samples of dilute metallic alloys are deformed under constant strain rate conditions. It is characterized by three types of bands and the associated stress serrations [28,29,42–46] observed with increasing strain rate or decreasing temperature. At the lower end of $\dot{\epsilon}_a$, randomly nucleated static type-C bands with large characteristic stress drops are seen. The serrations are quite regular. At intermediate $\dot{\epsilon}_a$, “hopping” type-B bands are seen where a new band is formed ahead of the previous one giving a visual impression of a hopping character. The serrations are more irregular with amplitudes that are smaller than that for type C. Finally, at high $\dot{\epsilon}_a$, the continuously propagating type-A bands associated with small stress drops are found. These bands have been shown to represent different correlated states of dislocations in the bands [33–37].

There are a number of models that target specific features of the PLC effect. These use local strains, strain rates, negative strain rate sensitivity of the flow stress, activation enthalpy of dynamic strain aging, waiting, etc. [40,47–51]. However, there are fewer models that predict the characteristic features of the three types of bands [34–37,50,51] required for calculating the associated AE spectra. Here, we use the AK model since it captures most generic features of the PLC effect, including the three types of bands and large number of features such as the existence of the instability within a window of strain rates, the negative strain rate behavior of the flow stress [39,52], the chaotic nature of stress drops at low strain rates [53], and the power-law distribution of stress drop magnitudes and durations [33,34,36,54–56]. In addition, the AK model has been recently shown to predict the Lüders-like band as well [33,34,36,37,39]. The basic idea of the model is that all of the qualitative features of the PLC effect emerge from the nonlinear interaction of a few collective degrees of freedom assumed to be represented by a few dislocation densities. The model consists of three types of densities, namely the mobile, immobile, and dislocations with solute atoms, denoted by $\rho_m(x,t)$, $\rho_{im}(x,t)$, and $\rho_c(x,t)$ respectively. The evolution equations for these densities in the unscaled form are

$$\frac{\partial \rho_m}{\partial t'} = -\beta \rho_m^2 - f \beta \rho_m \rho_{im} - \alpha_m \rho_m + \gamma \rho_{im} + \theta v_0 \left[\frac{\sigma_{\text{eff}}}{\sigma_y} \right]^m \rho_m + \frac{\Gamma \theta v_0}{\rho_{im}} \frac{\partial^2}{\partial x^2} \left[\frac{\sigma_{\text{eff}}}{\sigma_y} \right]^m \rho_m, \quad (18)$$

$$\frac{\partial \rho_{im}}{\partial t'} = \beta \rho_m^2 - p \beta \rho_m \rho_{im} - \gamma \rho_{im} + \alpha_c \rho_c, \quad (19)$$

$$\frac{\partial \rho_c}{\partial t'} = \alpha_m \rho_m - \alpha_c \rho_c. \quad (20)$$

All terms in Eq. (18) except the third and fourth terms have already been explained (see Sec. III A). The third term $\alpha_m \rho_m$ in Eq. (18) refers to solutes diffusing to mobile dislocations temporarily arrested by immobile (forest) dislocations. Thus, $\alpha_m \rho_m$ is the gain term for ρ_c . α_m is a function of the solute concentration C at the core of dislocations, D_c is the diffusion constant of the solute atoms, and λ is an effective attractive distance for the solute segregation. Then, $\alpha_m = \frac{D_c(T)C}{\lambda^2}$. As

dislocations progressively acquire more solute atoms, they slow down at a rate α_c and eventually stop, at which point they are considered as ρ_{im} . Thus, the loss rate $\alpha_c \rho_c$ in Eq. (20) is the gain term given by Eq. (19) for ρ_{im} . For the same reason, we consider ρ_{im} to include dislocations pinned by solute atmosphere as well. [Note the difference in the interpretation of ρ_{im} used in Eqs. (16) and Eq. (19).] Thus, the loss term $\gamma \rho_{im}$ in Eq. (19) is a gain term in Eq. (18). This term is considered to represent the unpinning of that fraction of immobile dislocations from the solute clouds. As in the model for continuous yield (Sec. III A), the spatial coupling [the sixth term in Eq. (18)] in this model arises from the double cross-slip process that allows dislocations to move into neighboring spatial elements. Equations (18)–(20) are coupled to the machine equation (17) that represents the constant strain rate deformation condition.

IV. COMPUTING ACOUSTIC EMISSION SPECTRUM DURING PLASTIC DEFORMATION

Now we consider the basic difficulty in describing slow plastic deformation and fast sound-wave propagation simultaneously. Experimental strain rates are in the range 10^{-6} – 10^{-2} s, while experimental AE frequencies are from KHz to MHz that differ by almost 10^8 – 10^{10} . This difference translates into the difference in the time steps for integration of the dislocation density equations (or $\dot{\epsilon}_p$) and the wave equations [Eqs. (8)–(12)]. For the sake of clarity, we use primed variable t' for the dislocation density evolution equations or for plastic strain rate $\dot{\epsilon}_p(k,t')$. Denoting the i th integration time step of $\dot{\epsilon}_p(k,t')$ (with k referring to spatial coordinate) by $\delta t'_i$, for the time interval between $t'_{i+1} < t' < t'_i$, we need to ensure that $\Lambda \delta t = \delta t'_i$ where δt is the step size used for Eqs. (8)–(12) and $\Lambda \gg 1$. Then, we should impose $\frac{\partial \dot{\epsilon}_p(k,t)}{\partial t} = \Lambda^2 \frac{\partial \dot{\epsilon}_p(k,t')}{\partial t'}$. Λ would be different for each type of the plastic deformation cases considered since the time step for integration for dislocation density evolution equations depends on whether or not they are stiff. However, for our purposes, it would be adequate to use the mean value of Λ . As for the spatial part, the wave equations and the dislocation density evolution equations are solved on the same spatial grid of 100 points (for $L = 0.05$ m). Further, since $\dot{\epsilon}_p(k,t')$ is calculated at much coarser time steps compared to Eqs. (8)–(12), we need to use interpolated values for $\dot{\epsilon}_p(k,t')$ in the source term. We now outline the steps used for obtaining the AE spectrum.

Step 1. Solve Eqs. (15)–(17) [or Eqs. (18)–(20) and (17) for the AK model] for the entire time interval and obtain $\dot{\epsilon}_p(k,t'_i)$ and $\sigma_a(t'_i)$ using a fixed or variable time step $\delta t'$ (as the case may be) for i, \dots, M and $k = 1, \dots, 100$.

Step 2. Start with $t = 0$ along with the stated initial and boundary conditions and solve Eqs. (8)–(12) for the interval $0 < t < t'_i$ corresponding to integration time step $\delta t'$ in Eqs. (15)–(17) [or Eqs. (18)–(20) and (17) for the AK model] for that interval. This gives $\epsilon_e(k,t)$ for $0 < t < t'_i$. Repeat integration for successive time steps.

Step 3. The stress $\sigma_e(t)$ obtained using $\epsilon_e(k,t)$ (and using the elastic modulus E for the sample) would, in principle, be different from that obtained from the machine equation (17), particularly in the plastic regime. Note also that we need to use

TABLE I. Parameter values used for the continuous yield model.

β (m ² s ⁻¹)	δ (m s ⁻¹)	f	v_0 (m s ⁻¹)	m
8.33×10^{-14}	5.4×10^{-11}	10^{-3}	10^{-7}	10

the interpolated values of $\dot{\epsilon}_p(k, t'_i)$ as an input into Eqs. (8)–(12).

Step 4. The dissipated acoustic energy is calculated using Eq. (7). We note here that the value of η is not known. However, from Eq. (2) [or Eq. (3)], we see $\eta/\rho \sim 1$, since $\eta/\rho \gg 1$ corresponds to the overdamped situation and $\eta/\rho \ll 1$ corresponds to the underdamped case. We have used a fixed value of η for the three cases so that the AE spectrum reflects the relative magnitudes.

We stress that the method for calculating the AE spectrum is approximate since Eq. (17) assumes equilibration to obtain plastic strain rate $\dot{\epsilon}_p(k, t')$. The method is akin to adiabatic schemes.

V. ACOUSTIC EMISSION SPECTRUM DURING A TYPICAL YIELD

Computation of the AE spectrum requires that we solve Eqs. (15)–(17) and use the plastic strain rate $\dot{\epsilon}_p(k, t')$ as the source term in Eqs. (8)–(12). Therefore, we first solve Eqs. (15)–(17) for the entire time interval to obtain $\dot{\epsilon}_p(k, t')$.

A. Numerical solution of model equations for continuous yield

We first estimate the orders of magnitudes of the model parameters. The parameter values of E^* , σ_y , b , and $\dot{\epsilon}_a$ are taken from the targeted experiment. Here, we attempt to predict the smooth $\sigma - \epsilon$ curve in Fig. 2(c) of Ref. [19] for which experimental parameters are $\sigma_y = 0.3$ GPa, $E^*/\sigma_y = 416$. (The value of $b = 0.25$ nm.) The experimental strain rate $\dot{\epsilon}_a = 1.67 \times 10^{-4}$ s. The theoretical parameter θv_0 constitutes a time scale which has been set to unity (one second) so that the plastic strain rate evolution time scale matches the experimental time scale. Other parameters, β, f, δ , are easily estimated by using typical asymptotic values of ρ_m and ρ_{im} that are in the range $\sim 10^{13}$ – 10^{14} m² [37]. The results presented here are for the parameter values given in Table I. The constant Γ is of the order of $1/\beta$ and hence $\Gamma \sim 10^{12}$. Equations (15)–(17) are solved on a grid of $N = 100$ points for a sample length $L = 0.05m$. The initial conditions used for $\rho_m(j, 0)$ and $\rho_{im}(j, 0)$ are taken to be uniformly distributed along the sample with a Gaussian spread of their values around a mean value 4.5×10^{11} m² and 10^{12} m², respectively. The variance for ρ_m is 1×10^{12} m² and that for ρ_{im} is 1×10^{11} m². The boundary conditions are $\rho_m(1, t') = \rho_m(N, t') \sim 10^{11}$ m² and $\rho_{im}(1, t') = \rho_{im}(N, t') = 10^{14}$ m². The high value for $\rho_{im}(N, t')$ represents the fact that the sample is strained at the grips. We have used “ode15s” MATLAB solver for the numerical solution. We shall use $\dot{\epsilon}_p(j, t')$ obtained as a source term in Eqs. (8)–(12) for the AE studies. However, since the step size needed for integrating Eqs. (8)–(12) is $\delta t \sim 0.001$, it requires that we supply the values of $\dot{\epsilon}_p(t')$ for intermediate times.

The calculated model stress-strain curve is shown in Fig. 2 along with experimental points extracted from Fig. 2(c) of [19].

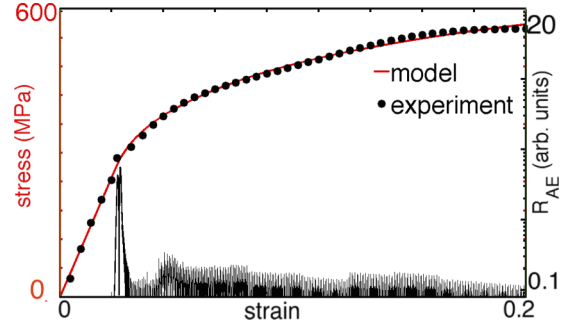


FIG. 2. (Color online) Stress-strain curve for a continuous yield (continuous curve) with experimental points (●) extracted from Fig. 2(c) of Ref. [19] for $\dot{\epsilon}_a = 1.67 \times 10^{-4}$ s along with the corresponding AE spectrum.

It is clear that the model $\sigma - \epsilon$ curve matches the experimental $\sigma - \epsilon$ quite well.

B. Acoustic emission spectrum

We have used $\dot{\epsilon}_p$ obtained from Eqs. (15)–(17) as a source term in Eqs. (8)–(12) to obtain the AE spectrum R_{AE} by using Eq. (7). This is shown in Fig. 2. This may be compared with the experimental AE spectrum for the continuous yield shown in Fig. 2(c) of Ref. [19]. It is clear that the overall shape of the model AE spectrum is quite similar to the experimental AE spectrum. Note that even though the $\sigma - \epsilon$ is smooth, the burstlike character of the predicted AE signals (and also the experimental AE signals) is reflective of the fundamentally intermittent nature of plastic deformation.

VI. ACOUSTIC EMISSION ACCOMPANYING THE DIFFERENT TYPES OF PLC BANDS

We first consider the solution of Eqs. (18)–(20) and Eq. (17), and discuss the features of different types of PLC bands and the associated serrations predicted by the AK model before computing the acoustic energy R_{AE} . To do this, we first estimate the parameters following the same procedure adopted for the earlier case (Sec. III A). Experimental parameters such as $\dot{\epsilon}_a$, E^* , b , and h are adopted from experiments. As for the theoretical parameters, the model time scale θv_0 is set to unity as for the previous case. The other parameters, $f, \beta, \gamma, \alpha_m$, and α_c , are fixed easily by providing the steady-state values of ρ_m, ρ_{im} , and ρ_c [37]. (Note that the steady state exists for these set of equations.) As for α_m , it is estimated by using $\alpha_m = \frac{D_c C}{\lambda^2}$. The exact values used are shown in Table II.

We solve Eqs. (18)–(20) and (17) by using an adaptive step size algorithm (ode15s MATLAB solver). The initial values of the dislocation densities are chosen much the same way as for

TABLE II. Parameter values used for the AK model.

E^* (GPa)	σ_y (GPa)	α_m (s ⁻¹)	α_c (s ⁻¹)	v_0 (m s ⁻¹)
48	0.2	0.8	0.08	10^{-7}
γ (s ⁻¹)	f	m	β (m ² s ⁻¹)	Γ
5×10^{-4}	1	3	5×10^{-14}	10^{12}

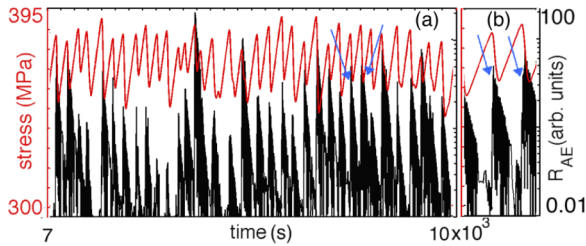


FIG. 3. (Color online) (a) Stress-strain curve for the randomly nucleated type-C bands and model acoustic energy R_{AE} plot for $\dot{\epsilon}_a = 1.125 \times 10^{-5}$ s. (b) Expanded portion of the AE spectrum shown between the arrows in (a).

the previous case. At the boundary, we use values that are two orders higher for $\rho_{im}(j, t')$ at $j = 1$ and N than the rest of the sample. Further, as bands cannot propagate into the grips, we use $\rho_m(j, t') = \rho_c(j, t') = 0$ at $j = 1$ and N .

A. The Portevin-Le Chatelier bands in the Ananthakrishna model

Earlier studies have demonstrated that the AK model predicts the three types of bands C, B, and A with increasing strain rate [33,34,36,37]. At low strain rates, uncorrelated static type-C bands are seen. The corresponding stress-time plot displays large-amplitude, nearly regular serrations as in experiments [28,29,42–46].

As $\dot{\epsilon}_a$ is increased, we see hopping type-B bands. The serrations are irregular and are of smaller magnitude. One important feature predicted by the model relevant to the AE studies is the correlation between the band propagation property and the small-amplitude serrations (SASs). In a recent study [37], it was demonstrated that *band propagation induces small-amplitude serrations that are bounded on both sides by large-amplitude stress drops*. Figure 4(a) shows two type-B bands marked AB and CD. The corresponding SASs induced by these two propagating bands are shown by the two sets of arrows AB and CD. This stretch of SASs is bounded on both sides by large-amplitude stress drops. The large stress drop

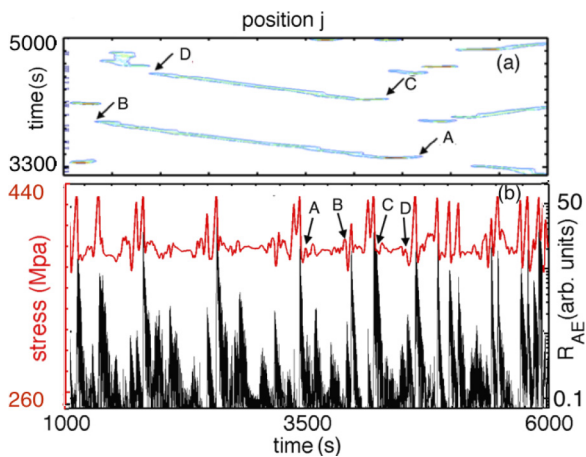


FIG. 4. (Color online) (a) Two partially propagating type-B bands for $\dot{\epsilon}_a = 3 \times 10^{-5}$ s. (b) The corresponding stress-strain curve and the model acoustic energy.

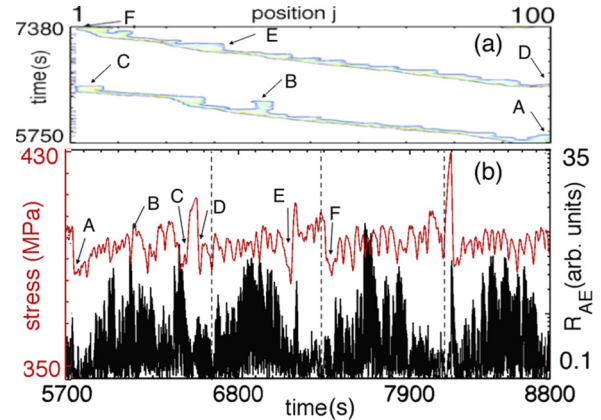


FIG. 5. (Color online) (a) Plots of two fully propagating type-A bands for $\dot{\epsilon}_a = 5.5 \times 10^{-5}$ s. (b) The corresponding stress-strain curve and the associated model acoustic energy R_{AE} .

at A is well correlated with the nucleation of the band AB. The one at B corresponds to stopping of the band. A similar observation holds for the band CD as well.

As we increase $\dot{\epsilon}_a$, the extent of propagation increases. Concomitantly, the duration of small-amplitude serrations increases. Typical contour plots of two type-A bands marked ABC and DEF are shown in Fig. 5(a) for $\dot{\epsilon}_a = 5.5 \times 10^{-5}$ s. The corresponding stretches of SASs induced by the propagating bands are marked by three sets of arrows marked ABC and DEF. While the spatial “width” of the propagating band is nearly uniform, occasionally one finds perturbations in the width. Two such points B and E are shown. At these points, we find relatively large-amplitude stress drops. Another feature is that the mean stress level of these SASs increases or decreases, as is clear for serrations A to B and C to D in Fig. 5(a). This feature is seen in many experimental $\sigma - \epsilon$ curves at high strain rates (see Fig. 1(c) for Cu-Al in Ref. [55]). As we shall see, these features have a direct influence on the nature of the AE spectrum.

B. Acoustic emission accompanying the three types of PLC bands

The calculated plastic strain $\dot{\epsilon}_p(k, t')$ for the entire time interval has been used as a source term in Eqs. (8)–(12) to obtain the model acoustic energy spectrum R_{AE} . A plot of R_{AE} along with the stress-time curve accompanying the type-C bands is shown in Fig. 3 for $\dot{\epsilon}_a = 1.125 \times 10^{-5}$ s. As can be seen, the bursts of acoustic emission appear at each stress drop and are well separated for strain rates $3 \times 10^{-6} < \dot{\epsilon}_a < 1.5 \times 10^{-5}$ s corresponding to the type-C bands. The postburst AE continuously decreases until a new AE burst appears. However, on an expanded scale, we find that there is a buildup of the AE signal from a low level just beyond the stress drop, as shown in Fig. 3(b). These features are confirmed by experimental AE spectra for the type-C bands [21,22].

With increasing $\dot{\epsilon}_a$, the AE bursts begin to overlap. In the region of partially propagating type-B bands, the AE spectrum consists of overlapping bursts leading to a low-amplitude continuous background. A typical plot of the AE spectrum for $\dot{\epsilon}_a = 3 \times 10^{-5}$ s is shown in Fig. 4(b). However, a

few large-amplitude AE signals can be seen overriding the continuous low-amplitude AE signals. Two observations can be made from the figure. First, the low-amplitude continuous AE signals are seen to be well correlated with the small-amplitude stress serrations induced by propagating bands. Second, the large-amplitude AE bursts are well correlated with the large-amplitude stress drops that are identified with the nucleation of new bands. Thus, large bursts of AE signal are correlated with the nucleation of new bands. This prediction is confirmed by recent experimental studies on AE during the PLC bands [21,22].

At high strain rates of the fully propagating type-A bands, the nature of the AE spectrum becomes fully continuous. A typical AE spectrum along with the stress-time curve for $\dot{\epsilon}_a = 5.5 \times 10^{-5}$ s is shown in Fig. 5(b). The figure shows that the AE spectrum is largely continuous, a feature that is consistent with the experimental AE spectrum [20–22]. Two other features are also evident. The AE spectrum exhibits occasional relatively large-amplitude AE signals overriding the continuous triangular-shaped AE spectrum. The relatively large burst of AE can be identified with the large-amplitude stress drops at points B and E on the stress-strain curve. We also see a correlation between these large bursts of AE with nucleation of the bands (A and D on the stress-time curve and C and F when the band reaches the sample end). This identification is similar to the type-B band nucleation. The overall triangular shape of the continuous AE signals (shown between the vertical dashed lines) is well correlated with the duration of increasing mean stress level of the SAS. It would be interesting to verify these correlations between band propagation induced small-amplitude serrations in the type-A band regime and the continuous AE spectrum.

The above discussion also shows that our approach predicts most of the features of the AE spectrum seen in experiments. It also provides insight into the origin of the low-amplitude continuous AE spectrum seen in both the type-B and type-A band regimes, namely, that it is directly correlated to the SASs induced by propagating bands. However, features associated with hardening, such as the decreasing activity with strain hardening, seen in experiments cannot be predicted within the scope of the AK model since the AK model does not include the forest hardening term.

VII. ACOUSTIC EMISSION DURING LÜDERS-LIKE PROPAGATING BAND

Before proceeding further, we briefly summarize the salient points about Lüders and show that the AK model predicts Lüders-like bands. Lüders bands traditionally refer to the propagating bands seen in polycrystalline samples following a yield drop. The bands propagate from one end to the other at practically zero hardening rate. The band propagation is ascribed to the incompatibility stresses between the grains. However, Lüders-like bands have been reported in many systems such as single crystals, alloys doped with solutes, irradiated single crystals, and even whiskers (see Ref. [27] for a review). According to Neuhäuser [27], the resistance offered by obstacles to dislocation motion is a common mechanism. The equivalent role of obstacles is played by solute atoms in the AK model.

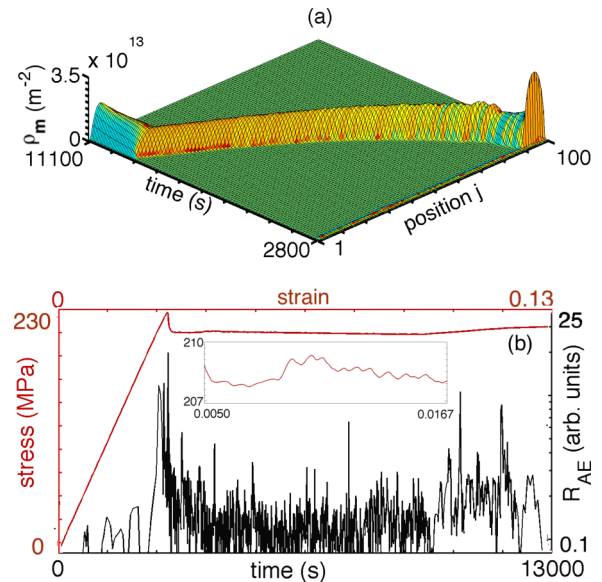


FIG. 6. (Color online) (a) A plot of the Lüders-like propagating band for $\dot{\epsilon}_a = 1.67 \times 10^{-6}$ s. (b) The corresponding stress-strain plot. The inset shows small-amplitude stress serrations not visible on the full scale of (b). The model acoustic energy R_{AE} is also shown.

It is known that alloys exhibiting the PLC effect often also exhibit Lüders regime [21,22,25]. Since the AK model exhibits most of the features of the PLC effect, including the three band types, it is conceivable that the AK model also exhibits Lüders-like bands. Indeed, the AK model has recently been shown to exhibit Lüders-like bands [37]. Figure 6(a) shows a Lüders-like band starting immediately after yield drop and traveling from one end to the other with a near constant velocity. The parameter values used are $\alpha_m = 1$ s, $\alpha_c = 0.002$ s, $\gamma = 5 \times 10^{-4}$ s, $E^*/\sigma_y = 240$, $m = 10$, and $\dot{\epsilon}_a = 1.67 \times 10^{-6}$ s. The corresponding stress-strain curve is shown in Fig. 6(b). It is clear that the stress level remains nearly constant at the lower yield value of ~ 200 MPa. While the stress-strain curve looks smooth on this scale, we do find small-amplitude serrations as shown in the inset.

Acoustic emission during Lüders-like band propagation

We have calculated the AE spectrum by following the same procedure as for the previous cases. This is shown in Fig. 6(b). As can be seen, the AE spectrum exhibits a peak corresponding to the yield drop. The AE activity rapidly decreases to a low level in the band propagation regime. Indeed, the decrease in the peak-level AE activity in the propagating region is consistent with experiments [21–23]. The peak in the AE spectrum at the yield is due to rapid multiplication of dislocations from a low initial density. The decrease in the AE activity during the band propagation can be identified with band propagation induced small-amplitude serrations shown in the inset of Fig. 6(b). Recall that the small-amplitude serrations induced during type-A band propagation were shown to be well correlated with low-amplitude continuous AE signals. In this case, the amplitude of the serrations is even smaller than the case of the type-A PLC band, typically less than 2 MPa, which is the primary cause of the low-level AE signals in the propagating region.

VIII. DISCUSSION AND CONCLUSIONS

In summary, we have developed a theoretical framework for describing the nature of the AE spectrum accompanying any plastic deformation and have illustrated the applicability to three distinct cases of plastic deformation. The dissipated AE energy is represented by the Rayleigh-dissipation function [4,6,7,10,11]. The plastic strain rate computed from the dislocation density evolution equations goes as a source term in the wave equation. The several orders of magnitude difference between the inertial time scale and the plastic deformation time scale is incorporated as a scale factor in the numerical solution of the wave equation. The necessity to impose mutually compatible boundary conditions between the wave equation and the dislocation density evolution equations forced us to deal with the discrete form of the wave equation.

The basic framework itself is independent of what kind of plastic deformation is targeted as long as the plastic strain rate as a function of space and time can be calculated using some method. However, the ability to construct the evolution equations for the dislocation microstructure matching the experimental features directly influences the resulting AE spectrum. It is therefore important to ensure that the model equations correctly predict the observed stress-strain curves and spatiotemporal features of the plastic deformation. Indeed, the good match between the model AE spectra and the experimental AE spectra in the three cases considered can only be attributed to the correctness in modeling the salient features of plastic deformation. The fact that the dislocation density based model closely reproduces the smooth experimental stress-strain curve and also the shape of the experimental AE spectrum should be taken as a validation of the correctness of the model. On the other hand, the burstlike character of the AE signals reflecting the fundamentally intermittent nature of plastic deformation is *more a validation of the correctness of the framework itself*. In the case of the PLC effect, the fact that the predicted AE spectra are consistent with the experimental AE spectra for each of the band types [18,20–22,25] is clearly due to the fact that the AK model predicts the three band types and associated serrations. The results show that the AE spectrum consists of well-separated bursts of AE occurring at every stress drop for the type-C bands. As $\dot{\epsilon}_a$ is increased towards the region of type-B bands, these bursts of AE tend to overlap, forming a low-level nearly continuous background. The AE spectrum corresponding to the type-A band is nearly continuous. The nature of the AE spectrum during Lüders-like band propagation predicted by the AK model is also consistent with experiments [21–23]. More importantly, our method is able to capture the intermittent burstlike character of the AE signals in all of the cases considered.

Interestingly, our approach is able to predict some details seen in the experimental AE spectrum, such as the unambiguous identification of a few large-amplitude AE signals with the nucleation of a new band [21,22]. More importantly, our study shows that the low-amplitude continuous AE spectrum seen in both the type-B and type-A band regimes and also the Lüders band are directly correlated with the small-amplitude serrations induced by propagating bands. Simultaneous measurement of band propagation, stress, and the associated AE spectrum should validate this result.

We now comment on the strengths and limitations of our approach. As stated above, the approach is general enough provided the plastic strain rate can be obtained from any model that captures the spatiotemporal features and stress-strain curve of the specific plastic deformation. From this point of view, the plastic strain rate obtained from Hähner [50] and Kok *et al.* [51] can be used to obtain the AE spectrum since these models predict the three PLC bands. The approach can also be applied to other types of plastic deformations not considered here. For example, the AE technique has been used to study a variety of modes of plastic deformation such as load-rate controlled PLC experiments [57], cyclic loading experiments [58], and stress relaxation experiments [22]. Our method is applicable to these cases since the dislocation evolution equations can be coupled to load-rate controlled and cyclic loading conditions instead of the constant strain rate deformation [59]. The method can also be used for the case of AE studies in nano- and microindentation experiments [60] since a dislocation dynamical model for nanoindentation has been developed recently [61].

Lastly, consider the importance of modeling dislocation evolution equations. In alloys exhibiting the PLC effect, serrations are seen on stress-strain curves that display strain hardening. Experiments show that the AE activity decreases with increasing strain. This feature cannot be predicted by the present form of the AK model since it includes hardening only in a marginal way. However, the strain hardening feature is recovered once the forest hardening term $\rho_m \rho_{im}^{1/2}$ is included in the AK model [62]. Therefore, we expect that the revised AK model should recover the AE features that depend on strain hardening. Work in this direction is in progress.

One last example is the case of acoustic emission during crack propagation [63,64]. During crack propagation in ductile materials, plastic deformation blunts the crack tip. Clearly, it should be possible to adopt our framework by using equations that describe dynamic propagation of a crack. Even in the case of brittle fracture propagation, it should be possible to adopt our method since brittle fracture can be viewed as a limiting case of ductility.

A comment is in order about the algorithm followed in computing the AE spectrum. The acoustic energy spectrum was calculated using the plastic strain rate computed from dislocation-based models along with the machine equation (17). However, Eq. (17) assumes stress equilibration. This was done for the sake of convenience of computation. The framework itself is more general since the elastic strain can be obtained from the wave equation which can be used to obtain the unrelaxed stress. Work in this direction is in progress.

While our approach to acoustic emission is phenomenological, recently the phase field crystal (PFC) model [65] has been used to predict the power-law distribution of AE signals. Since the model has the ability to deal simultaneously with elastic and defect degrees of freedom, it may have potential for AE studies. However, the ability of the PFC model to predict the generic features of specific cases of plastic deformation such as the stress-strain curve and the associated spatiotemporal features (such as the three types of PLC bands and Lüders band or even smooth stress-strain curve) remains to be established since the characteristic features of the AE spectrum are directly correlated with these features.

ACKNOWLEDGMENTS

G.A. acknowledges the Board of Research in Nuclear Sciences Grant No. 2012/36/18-BRNS and the support from

the Indian National Science Academy through the Senior Scientist position. Part of this work was carried out when J.K. and R.S. were at the Indian Institute of Science and both were supported under the BRNS grant.

-
- [1] P. Diodati, F. Marchesoni, and S. Piazza, *Phys. Rev. Lett.* **67**, 2239 (1991).
- [2] D. A. Lockner, J. D. Byerlee, V. Ponomarev, and A. Sidorin, *Nature (London)* **350**, 39 (1991).
- [3] A. Petri, G. Paparo, A. Vespignani, A. Alippi, and M. Costantini, *Phys. Rev. Lett.* **73**, 3423 (1994).
- [4] Rumi De and G. Ananthakrishna, *Europhys. Lett.* **66**, 715 (2004).
- [5] E. Vives, I. Ràfols, L. Mañosa, J. Ortín, and A. Planes, *Phys. Rev. B* **52**, 12644 (1995).
- [6] R. Ahluwalia and G. Ananthakrishna, *Phys. Rev. Lett.* **86**, 4076 (2001).
- [7] S. Sreekala and G. Ananthakrishna, *Phys. Rev. Lett.* **90**, 135501 (2003).
- [8] D. Maugis and M. Barquins in *Adhesion 12*, edited by K. W. Allen (Elsevier, London, 1988), p. 205.
- [9] M. Ciccotti, B. Giorgini, D. Villet, and M. Barquins, *Int. J. Adhes. Adhes.* **24**, 143 (2004).
- [10] Rumi De and G. Ananthakrishna, *Phys. Rev. Lett.* **97**, 165503 (2006).
- [11] Jagadish Kumar, R. De and G. Ananthakrishna, *Phys. Rev. E* **78**, 066119 (2008).
- [12] M. C. Miguel, A. Vespignani, S. Zapperi, J. Weiss, and J-R. Grasso, *Nature (London)* **410**, 667 (2001).
- [13] J. Weiss and D. Marsan, *Science* **299**, 89 (2003).
- [14] Jagadish Kumar and G. Ananthakrishna, *Phys. Rev. Lett.* **106**, 106001 (2011).
- [15] V. R. Skal's'kyi, O. E. Andreikiv, and O. M. Serhienko, *Mater. Sci.* **39**, 86 (2003).
- [16] H. Dunegan and D. Harris, *Ultrasonics* **7**, 160 (1969).
- [17] D. R. James and S. H. Carpenter, *J. App. Phys.* **42**, 4685 (1971).
- [18] C. H. Caceres and Rodriguez, *Acta Metall.* **35**, 2851 (1987).
- [19] Z. Han, H. Luo, and H. Wang, *Mater. Sci. Eng. A* **528**, 4372 (2011).
- [20] F. Zeides and J. Roman, *Scr. Metall. Mater.* **24**, 1919 (1990).
- [21] F. Chmelík, A. Ziegenbein, H. Neuhäuser, and P. Lukáč, *Mater. Sci. Eng. A* **324**, 200 (2002).
- [22] F. Chmelík, F. B. Klose, H. Dierke, J. Šachl, H. Neuhäuser, and P. Lukáč, *Mater. Sci. Eng. A* **462**, 53 (2007).
- [23] T. V. Murav'ev and L. B. Zuev, *Technol. Phys.* **53**, 1094 (2008).
- [24] A. A. Shibkov and A. E. Zolotov, *Crystalogr. Rep.* **56**, 141 (2011).
- [25] I. V. Shashkov, M. A. Lebyodkin, and T. A. Lebedkina, *Acta Mater.* **60**, 6842 (2012).
- [26] M. D. Uchic, P. A. Shade, and D. M. Dimiduk, *Ann. Rev. Mater. Res.* **39**, 361 (2009).
- [27] H. Neuhäuser, in *Dislocations in Solids*, Vol. 6, edited by F. R. N. Nabarro (North Holland, Amsterdam, 1983).
- [28] G. Ananthakrishna, *Phys. Rep.* **440**, 113 (2007).
- [29] A. Yilmaz, *Sci. Technol. Adv. Mater.* **12**, 063001 (2011).
- [30] K. Malen and L. Bolin, *Phys. Stat. Sol. (B)* **61**, 637 (1974).
- [31] B. Tirbonod, *Int. J. Fracture* **58**, 21 (1992).
- [32] B. Polyzos and A. Trochidis, *Wave Motion* **21**, 343 (1995).
- [33] M. S. Bharathi and G. Ananthakrishna, *Europhys. Lett.* **60**, 234 (2002).
- [34] M. S. Bharathi and G. Ananthakrishna, *Phys. Rev. E* **67**, 065104(R) (2003).
- [35] M. S. Bharathi, S. Rajesh, and G. Ananthakrishna, *Scr. Mater.* **48**, 1355 (2003).
- [36] G. Ananthakrishna and M. S. Bharathi, *Phys. Rev. E* **70**, 026111 (2004).
- [37] Ritupan Sarmah and G. Ananthakrishna, *Acta Mater.* **91**, 192 (2015).
- [38] L. D. Landau and E. M. Lifschitz, *Theory of Elasticity* (Pergamon, Oxford, 1986).
- [39] G. Ananthakrishna and M. C. Valsakumar, *J. Phys. D* **15**, L171 (1982).
- [40] L. P. Kubin and Y. Estrin, *Acta Metall. Mater.* **38**, 697 (1990).
- [41] D. Hull and D. J. Bacon, *Introduction to Dislocations* (Butterworth-Heinemann, Oxford, 2007).
- [42] K. Chihab, Y. Estrin, L. P. Kubin, and J. Vergnol, *Scr. Metall.* **21**, 203 (1987).
- [43] N. Ranc and D. Wagner, *Mater. Sci. Eng. A* **394**, 87 (2005).
- [44] N. Ranc and D. Wagner, *Mater. Sci. Eng. A* **474**, 188 (2008).
- [45] Z. Jiang, Q. Zhang, H. Jiang, Z. Chen, and X. Wu, *Mater. Sci. Eng. A* **403**, 154 (2005).
- [46] H. Jiang, Q. Zhang, X. Chen, Z. Chen, Z. Jiang, X. Wu, and J. Fan, *Acta Mater.* **55**, 2219 (2007).
- [47] P. Penning, *Acta Metall.* **20**, 1169 (1972).
- [48] P. G. McCormic, *Acta Metall.* **36**, 3061 (1988).
- [49] U. F. Kocks, in *Progress in Materials Science*, edited by X. Ashby *et al.*, Chalmers Anniversary Vol. (Pergamon, Oxford, 1981).
- [50] P. Hähner, A. Ziegenbein, E. Rizzi, and H. Neuhäuser, *Phys. Rev. B* **65**, 134109 (2002).
- [51] S. Kok, M. S. Bharathi, A. J. Beaudoin, G. Ananthakrishna, S. Fressengeas, L. P. Kubin, and M. Lebyodkin, *Acta Mater.* **51**, 3651 (2003).
- [52] S. Rajesh and G. Ananthakrishna, *Phys. Rev. E* **61**, 3664 (2000).
- [53] G. Ananthakrishna and M. C. Valsakumar, *Phys. Lett. A* **95**, 69 (1983).
- [54] S. J. Noronha, G. Ananthakrishna, L. Quaouire, C. Fressengeas, and L. P. Kubin, *Int. J. Bifurcation Chaos Appl. Sci. Eng.* **7**, 2577 (1997).
- [55] G. Ananthakrishna, S. J. Noronha, C. Fressengeas, and L. P. Kubin, *Phys. Rev. E* **60**, 5455 (1999).
- [56] M. S. Bharathi, M. Lebyodkin, G. Ananthakrishna, C. Fressengeas, and L. P. Kubin, *Phys. Rev. Lett.* **87**, 165508 (2001).
- [57] P. Dobroň, J. Bohlen, F. Chmelík, Lukáč, D. Letzig, and K. U. Kainber, *Mater. Sci. Eng. A* **462**, 307 (2007).

- [58] T. T. Lamark, F. Chmelík, Y. Estrin, and Lukáč, *J. Alloys Compd.* **378**, 202 (2004).
- [59] M. V. Glazov, D. R. Williams, and C. Laird, *Appl. Phys. A* **64**, 373 (1997).
- [60] N. J. Tymiak, A. Daugela, T. J. Wyrobok, and O. L. Warren, *J. Mater. Res.* **18**, 784 (2003).
- [61] G. Ananthakrishna, R. Katti, and Srikanth K., *Phys. Rev. B* **90**, 094104 (2014).
- [62] Ritupan Sarmah, Ph.D thesis, Indian Institute of Science, Bangalore, India, 2012.
- [63] K. Ravi-Chandar, *Dynamic Fracture* (Elsevier, Boston, 2004).
- [64] L. B. Freund, *Dynamic Fracture Mechanics* (Cambridge University Press, Cambridge, 1998).
- [65] P. Y. Chan, G. Tsekenis, J. Dantzig, K. A Dahmen, and N. Goldenfeld, *Phys. Rev. Lett.* **105**, 015502 (2010).